Sound & Vibration 2026, 60(2), 3889.
doi: https://doi.org/10.59400/sv3889

Article

Design optimization and comparative evaluation of oval and toroidal propeller geometries versus a conventional propeller

Rayn Nasr[1], Majd Shreif[2], Enrico Abou Jaoude[2], Celine Ahmar[2], Jihad Rishmany[2,*]

[1] Department of Aerospace Science and Technology, Politecnico di Milano, 20156 Milan, Italy

[2] Department of Mechanical Engineering, Faculty of Engineering, University of Balamand, Tripoli P.O. Box 100, Lebanon

*** Corresponding author:** Jihad Rishmany, jihad.rishmany@balamand.edu.lb

CITATION

Nasr R, Shreif M, Jaoude EA, et al. Design optimization and comparative evaluation of oval and toroidal propeller geometries versus a conventional propeller. Sound & Vibration. 2026; 60(2): 3889. https://doi.org/10.59400/sv3889

ARTICLE INFO

Received: 5 January 2026
Revised: 12 February 2026
Accepted: 6 March 2026
Available online: 11 March 2026

Abstract: Drones are increasingly used in delivery, aerial imaging, search and rescue, and agricultural monitoring due to their low cost, low emissions, and ability to reach hazardous or hard-to-access locations. However, a major limitation is the high noise produced by conventional propellers as they interact with the air. Recently, toroidal propellers have emerged as a promising alternative, offering aerodynamic benefits that can reduce noise while maintaining or improving thrust generation. This study investigates the performance of toroidal propellers, both circular and oval, compared to a conventional propeller. The assessment focuses on thrust production, efficiency, and noise emission using both experimental testing and numerical simulations. Results indicate that toroidal propellers provide notable advantages. Experiments showed approximately a 15 dB noise reduction and up to a fourfold increase in thrust relative to the conventional design. Simulations revealed that the oval toroidal propeller achieved the lowest noise level at 29.54 dB, while the circular design produced higher noise but delivered the greatest thrust, reaching 44.08 N. Overall, the study demonstrates that toroidal propellers can significantly enhance drone performance. The optimal choice between oval and circular designs depends on specific mission requirements, balancing noise reduction against thrust demand.

Keywords: toroidal propellers; aeroacoustics; propeller geometry optimization; aerodynamic performance analysis; noise reduction in unmanned aerial vehicles (UAVs); thrust efficiency; computational fluid dynamics (CFD)

1. Introduction

Drones were first developed for military applications but have since grown and advanced rapidly and entered the consumer market. They were initially used as weapons in the form of remote-guided air-borne missile deployments.

In 2024, the commercial drone market had a value of USD 30.02 billion. Analysts predict that this market will grow at an annual rate of 10.6% from 2025 to 2030. This expansion happens because businesses are using drones more and more in their daily activities. Numerous drone manufacturers are constantly experimenting, developing and improving solutions for a range of industries and uses, such as emergency response and videography [1].

However, the growing number of drone operations raises serious concerns about their potential to contribute to noise pollution. Drone sound causes higher irritation compared to airplane sounds or traffic sounds at identical volumes, where

certain acoustic properties were shown to have caused the disturbance, specifically high-frequency broadband sound plus the clear tones created by drones [2].

Similarly, investigations were conducted to compare sounds emitted by drones to those of vehicles and trucks. The researchers observed that people considered the sounds of drones more annoying than the sounds of cars, even when the sound level was equivalent. The study suggested that drone businesses could see community opposition in case drone sounds seem disruptive or exceed the loudness of noises from regular delivery vehicles, and therefore there is a need to assess the possibility to reduce this noise or at least change its frequency, aiming to make it less annoying [3].

The primary source of a drone's noise is the drone's propellers. Sound is generated when the propeller blades rotate and interact with the surrounding air, creating turbulent flow patterns. The major source of that noise is the tip vortices, where they play an important role in the noise generating process. These vortices become more pronounced as the blades spin faster, which results in an increase in the volume of the drone. Although propellers are crucial for producing the force required for flight, their acoustic characteristics provide a significant obstacle to drone adoption, especially in areas where noise is a concern, meaning that thrust and noise have a proportional relationship [4].

Classic propellers, also known as axial-flow propellers, are the most commonly used. Their design is based on the principles of helical lifting surfaces, where the blades generate thrust by inducing a pressure difference between the forward and rearward sides, but to improve the aerodynamic and noise characteristics a group of researchers at Massachusetts Institute of Technology created a toroidal propeller. Toroidal propellers represent a more innovative and promising approach. It consists of an enclosed-loop blade arrangement. In contrast to traditional blades, the toroidal propeller's continuous loop greatly lowers drag and decreases the creation of tip vortices. Thus, there might be a solution for drone operations that are quieter because of the associated aerodynamic enhancements that reduce noise emissions. Circular and oval designs are among the most common types of toroidal blades [5].

Ghoreyshi et al. [6] showed that oval-shaped propeller tips produce less noise than conventional round-tip propellers. The noise reduction came from better vortex control techniques and the elimination of tip vortex noises. Studies show that propeller designs that implement oval tips demonstrate quieter operation standards, and this feature benefits UAVs that need to operate in noise-sensitive conditions. Additional research carried out in propellers furthermore proved that toroidal blades generate wake vortex having a structure that minimizes noise production by creating a smooth flow that dissipates high-energy vortices that normally cause noise emissions, confirming the fact that toroidal propellers outperform conventional ones when it comes to noise generation [7].

CFD analysis between oval-tip toroidal propellers and circular-tip toroidal propellers, tested at different rotational speeds (RPMs) with varying blade count was conducted [3, 4, 8]. The 3-blade configuration proved to be the best design through research because it delivered the highest thrust-to-efficiency ratio at all RPMs tested. The oval-tip design outperformed the circular-tip propellers through better

flow behavior and reduced cavitation rates because oval shapes exhibit superior aerodynamic efficiency and noise reduction capacity [9].

In this study, the circular toroidal propeller was defined as the one with a symmetric ring shape, and the oval toroidal propeller as having an elongated or elliptical loop. Since there is limited literature comparing these configurations, simulations are conducted to assess the geometry effect on thrust and noise generation.

Recent work has strengthened the evidence on why drone noise is considered as unusually annoying and how this should affect both design criteria and assessment methods. Controlled listening studies show that, at comparable exposure levels, unmanned aerial system (UAS) sounds higher annoyance than conventional transport noise, with tonality, sharpness, and impulsive characteristics identified as dominant perceptual drivers [10–12]. Perception has also been shown to depend strongly on contextual soundscapes and individual listener sensitivity, motivating assessment approaches that extend beyond single-number sound pressure level metrics [13, 14]. From an engineering perspective, recent reviews highlight the need for integrated noise prediction and mitigation frameworks that couple validated experiments with high-fidelity numerical models for UAS [15, 16]. Advances in rotor and propeller aeroacoustics, including improved tonal-noise modeling and experimental–computational cross-validation, have enabled more reliable identification of geometry- and operating-condition-dependent noise mechanisms [17–19]. These developments support the present study's focus on how toroidal propeller geometry influences thrust and flow features linked to noise generation, while encouraging evaluation using perceptually relevant metrics rather than overall sound levels alone.

This paper offers a comparison between toroidal and conventional propeller designs to enhance optimization efforts. Through these objectives, the study advances toroidal propeller technology and provides significant insights for engineering applications in the marine, aerospace, and other industries.

2. Materials and methods

2.1. Propellers CAD modelling

All toroidal propeller designs were modeled using Solid Works, as for the conventional propeller a blueprint of the official DJI F450 was used directly to assist in the comparison process, and all measurements related to motor mounting were also taken from the official manual [8]. The model was scaled to have a span of 25 cm in order to match the tested model for comparison. The conventional one was assumed to have already been optimized, being a standard one used by the company.

2.1.1. Circular toroidal propeller modeling

The modeling of the circular toroidal is considered relatively easy, where its cross-section is basically formed by two concentric circles (**Figure 1a**). The diameter of the external circle was chosen to match the span-length requirement, whereas **Figure 1b** shows the pitch angle, which was the design parameter in the study. The thickness was set to 3 mm, mainly optimized for structural integrity and mass reduction, where going below that value could lead to the blade's failure and higher thickness would

significantly increase the overall mass, reducing the motor performance.

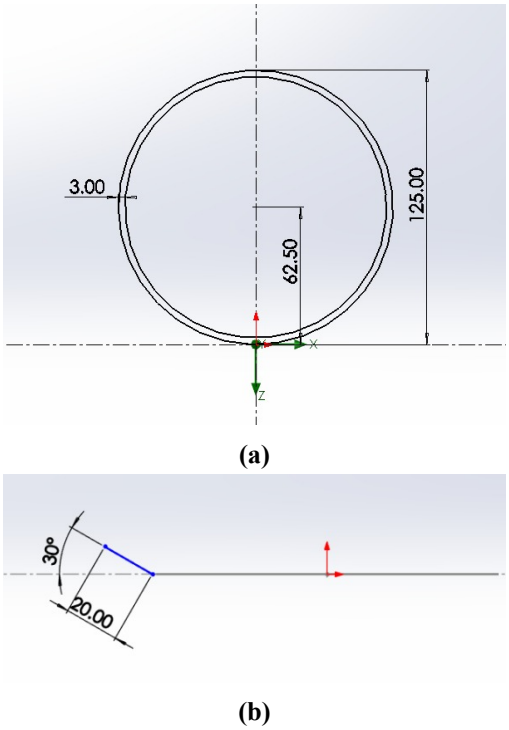

Figure 1. Modeling steps of the circular toroidal propeller (dimensions are in mm), **(a)** Cross section; **(b)** Pitch angle of the blade.

The structural optimization of the circular toroidal propeller was primarily focused on achieving a critical balance between mechanical integrity and mass reduction to ensure operational feasibility. A key optimization parameter was the 3 mm blade thickness, which was selected to prevent structural failure while avoiding excessive mass that would degrade motor performance. To further enhance structural stability and ensure smooth operation, the center of mass was precisely aligned with the concentric circles of the cross-section, which is essential for minimizing imbalances and vibrations during high-speed rotation. The selection of 3D-printed resin provided high material strength for the prototypes. However, despite these design optimizations, experimental trials indicated that the circular configuration lacked sufficient resistance to the centrifugal forces and structural stresses encountered when the motor was engaged, leading to blade failure. Future structural optimization could involve material substitution with high-performance composites or a recalibration of the thickness-to-drag ratio to better withstand high-RPM operational loads without compromising the propeller's inherent acoustic advantages.

Figure 2a shows the fully developed circular toroidal propeller, in addition to the center of mass that is perfectly aligned in the center of the circles, knowing that it is crucial to have a smooth operation without imbalances and vibrations. **Figure 2b** shows the 3D printed with a resin material for extra strength, the same material was also used for the oval one.

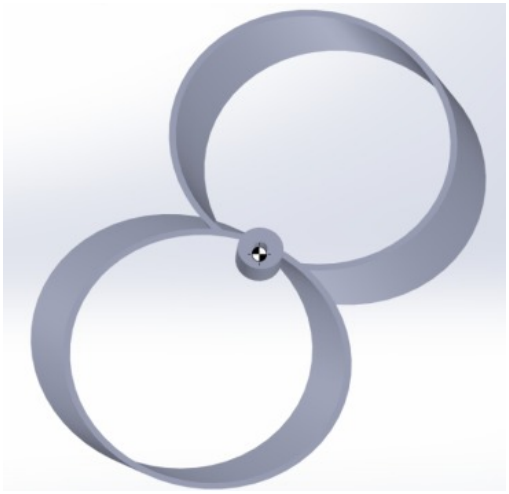

(a)

(b)

Figure 2. Fully developed circular toroidal propeller, **(a)** CAD model; **(b)** Manufactured blade.

2.1.2. Oval toroidal propeller modeling

The geometry of the oval shaped propeller is much more complex and is subjected to many variations. It is basically formed by two blades on each side, each having the same airfoil, and joined at the tip to reduce vortices. The varying parameters in this type of propeller could be the airfoil, the pitch angle, and the joint shape at the tip. In this study, the main focus is on varying the pitch angle while keeping all other parameters fixed.

In **Figure 3a** the details of the airfoil at the base of the propeller blade are shown in addition to the pitch angle. However, it is not directly an angle as in the circular case, but the vertical direction, having in this case a value of 3 mm, whereas by changing that dimension the airfoil will rotate by a certain angle which will be determined later. **Figure 3b** demonstrates the airfoil in the mid-section and the varying parameter here will also be the vertical dimension having a value of 4 mm. The blade tends to decrease its pitch angle as it gets closer to the tip, where at the mid-section, the angle is lower than that at the base by a value of 5°, in order to have a more uniform lift distribution since the velocity increases radially towards the tip. Finally, **Figure 3c** reveals the shape of a critical element in a toroidal propeller, which is the part that joins the blades together; however, in this paper this parameter was fixed to the value shown in the figure. The final step was to scale the propeller in order to have a 25 cm blade span.

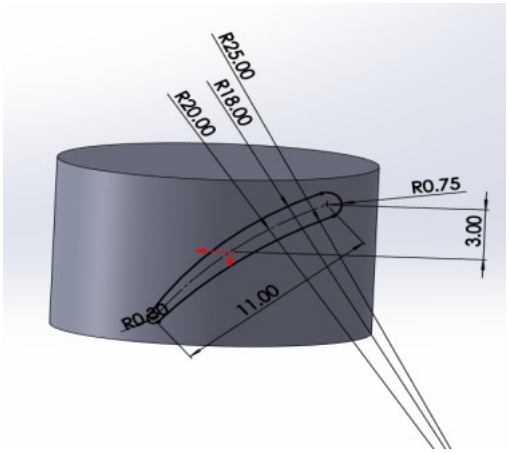

(a)

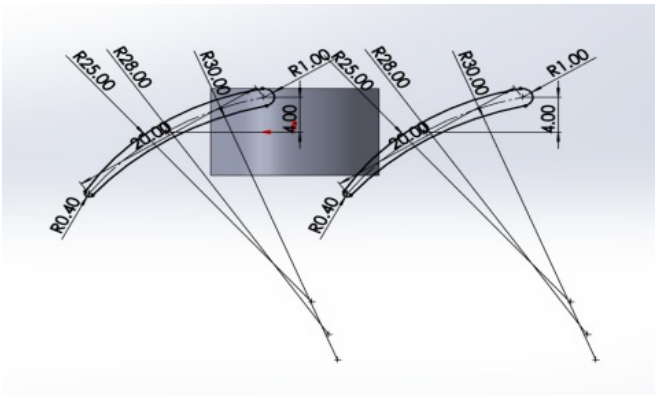

(b)

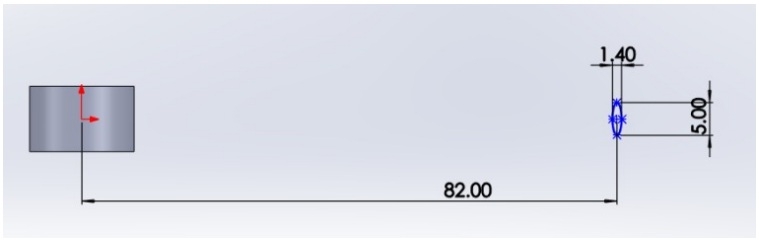

(c)

Figure 3. Modeling steps of the oval toroidal propeller (all dimensions are in mm), **(a)** Airfoil at the base of each blade; **(b)** Second airfoil placed in the mid-section of each blade; **(c)** Tip joint between the two blades.

Figure 4a demonstrates the fully designed circular toroidal propeller, while **Figure 4b** shows the manufactured propeller which was used for experimental testing.

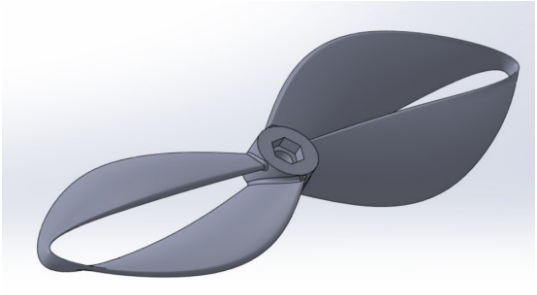

(a)

Figure 4. *Cont.*

(b)

Figure 4. Fully developed oval toroidal propeller, **(a)** CAD model; **(b)** Manufactured blade.

2.2. Computational fluid dynamics simulation

The goal of this study is to check the variation of the noise emitted by the rotating propeller and to compare the two toroidal models to the conventional one. However, to be able to identify the optimum design, the optimal configuration of each one has to be identified first and then compared against each other. As previously mentioned, the only variable was the pitch angle, where basically the same simulation was carried out with different angle values. The simulations had an angle increase of 5° between each iteration, establishing a theoretical range of [0°, 85°]. However, practical constraints necessitated the exclusion of certain angles. For the circular configuration, the study began at 10° and extended to a maximum of 60°. The lower bound was chosen because, at 0°, the blade, lacking camber, would behave like a flat plate, and at 5°, thrust generation was negligible; thus, both angles were disregarded. The upper limit was restricted to 60° in order to avoid stall effects, which would otherwise result in a significant reduction in motor efficiency.

For the oval toroidal configuration, the primary constraints were geometric rather than aerodynamic. Unlike the circular design, the cambered airfoil allowed the blade to generate thrust even at 0°. However, with the selected airfoil shown in **Figure 3b**, reducing the angle below 5° would result in blade overlap. The maximum angle was limited to 50° due to geometric issues, as the blade length would otherwise exceed the base dimensions. These limitations were imposed because the base was fixed according to the specifications of the motor intended for the experimental procedure, ensuring compliance with the propeller mounting size and measurements.

2.2.1. Initial parameters

Before launching the simulation, some parameters were fixed across all propellers. The physical feature of the simulation was selected as “local region averaging rotation”, flow characteristics were chosen to be laminar and turbulent, as for the pressure and temperature, they were set as the conventional at sea level.

2.2.2. Simulation goals and plots

The choice of plots and goals during the simulation setting process is set according to the desired results (**Figure 5**), and the chosen surface is that of the propeller blades.

Figure 5. CFD simulation goals set-up.

The most relevant goals for this study are the "Normal Force (Y)" representing the thrust generated from the propeller, the "Normal Force (X) and (Z)" representing the components of the force in the orthogonal plane with respect to the thrust vector, which basically is the resistance force applied on the propeller and countering the torque generated by the motor. The friction forces computed in the same plane were equivalent to the normal force; they were added with the sole purpose of double checking the results. Regarding the results at the acoustic level, two main plots were used (**Figure 6**).

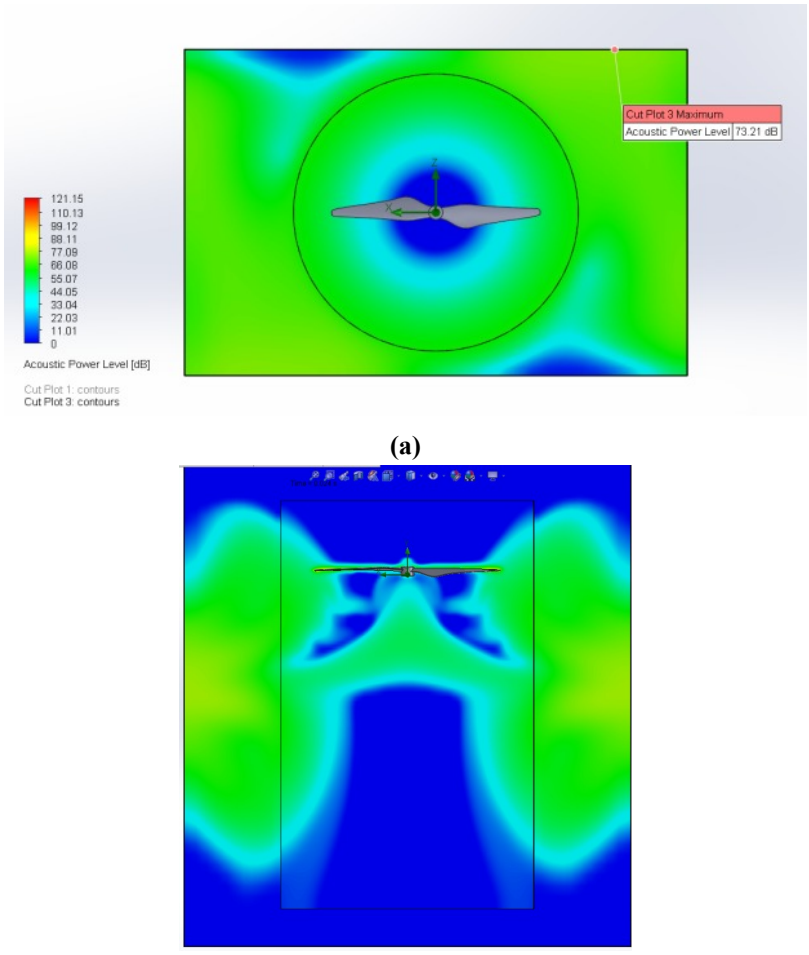

(a)

(b)

Figure 6. Cut plot of the acoustic power level for the conventional propeller, **(a)** at 25 cm distance below the propeller; **(b)** in the plane of the thrust vector.

2.2.3. Choosing the rotational and computational domains

The process of choosing the rotational and computational domains for the simulation is crucial in order to obtain accurate results. Having a small domain will lead to misleading values and inaccurate flow trajectory. In the case of overly large domains, the results would still be correct and accurate; however, this would require much more computational resources for each iteration. Therefore, a trade-off should be made between having domains as small as possible while maintaining a certain level of accuracy. Concerning the rotational domain, its diameter was constrained by the diameter of the propeller, where it must be slightly greater than the blade span (**Figure 7**), which was inspired by multiple propeller CFD studies [7,20].

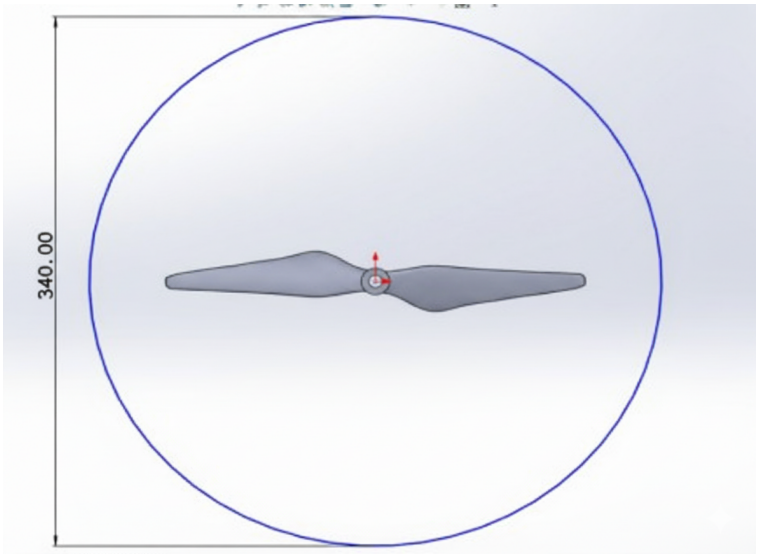

Figure 7. Diameter of the rotational domain.

An iterative approach was employed to determine both parameters. The iterations were carried out using the conventional propeller, allowing the obtained values to be directly compared with those provided in the motor and propeller specifications manual [8]. The rotational speed was set to the maximum RPM of the motor, which would result in the maximum thrust generated, which is around 9.8 N. The iterations were initially performed with a relatively coarse mesh and refined progressively, and the results were compared to the manufacturer's value.

The first iteration (**Figure 8a**) with a small computational domain and a short rotational one, shows that the air particles do not behave as expected (**Figure 8b**), since no vortices generated underneath the propeller. The turbulent air on the side of the propeller by itself shows that this set of rotational and computational domains will lead to inaccurate results.

Consequently, the subsequent iteration (**Figure 9a**) encompassed significantly larger domains to predict a more realistic behavior. From the cut plot in **Figure 9b**, it can be deduced that the domains are larger than required. The plot indicates where the air started to change direction and was unable to overcome the adverse gradient that indicates the free stream, and anything beyond that point would be beyond the scope and concern of this study.

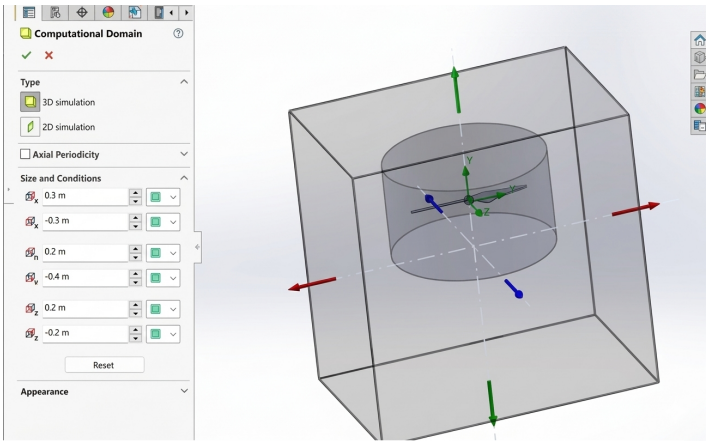

(a)

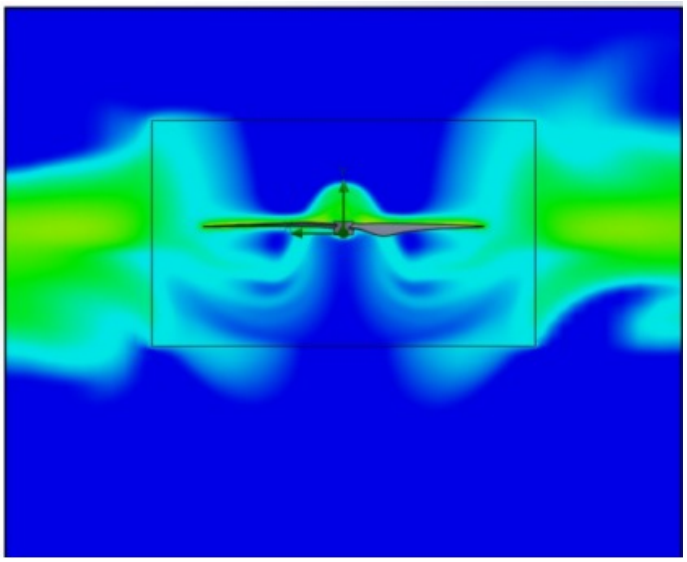

(b)

Figure 8. Characteristics and results of the First trial with the smallest domain, **(a)** Characteristics of the computational domain; **(b)** Cut plot results.

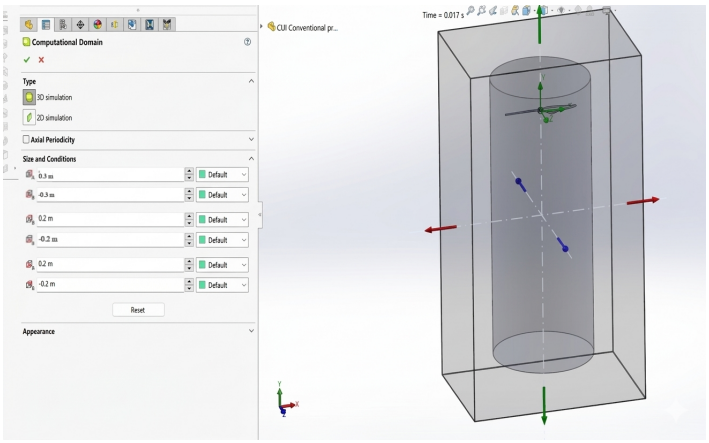

(a)

Figure 9. *Cont.*

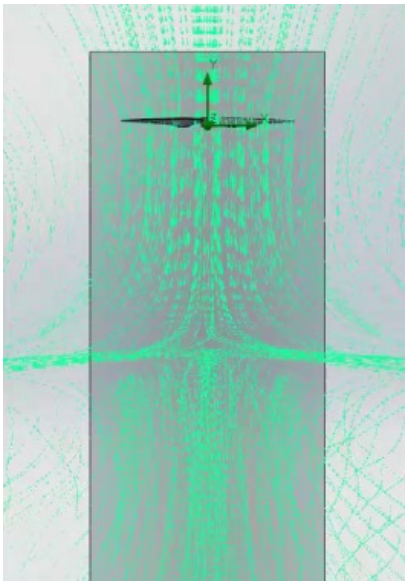

(b)

Figure 9. Characteristics and results of the trial with the biggest domain, **(a)** Characteristics of the computational domain; **(b)** Flow trajectories of the air particles.

From these results, other iterations that had the rotational and computational domains below the free stream location were developed, and in the end the rotational domain was set to a length of 450 mm underneath the propeller, corresponding to a location right below the free stream location, and the computational domain was set following the characteristic shown in **Figure 10**. Finally, a simulation using a finer mesh confirmed that these two domains yield results closely aligned with the values specified by the manufacturer in the manual [8].

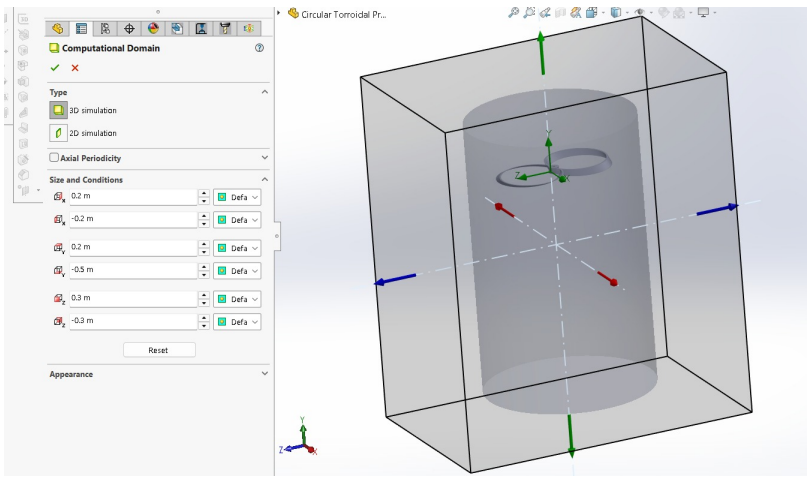

(a)

Figure 10. *Cont.*

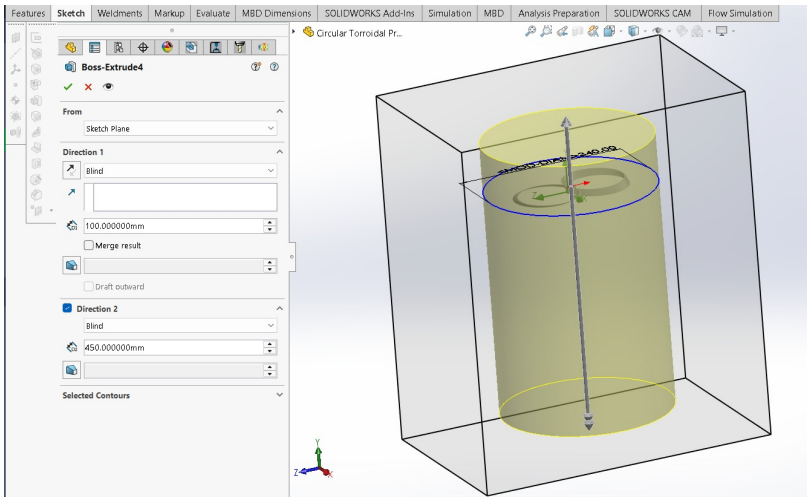

(b)

Figure 10. Final model characteristics, **(a)** Computational domain; **(b)** Rotational domain.

2.2.4. Mesh independency study

The next aspect to address was the mesh, as it plays a critical role in ensuring the accuracy of the simulation results. The method of mesh independence study was adapted to set an accurate mesh with the least computational power demand. The method relied on multiple iterations, where the first iteration had a coarse mesh and then progressively refined it after each step. After every trial, the results were plotted on a graph, and once a constant value was reached and the trend line started to act asymptotically, instead of random oscillating behavior, this indicated that the selected mesh was sufficient to get the correct results without any need to further increase it. In general, the mesh was not uniformly distributed; it was more concentrated in the center of the propeller. In addition, a finer setting was selected in the thrust vector plane compared to the other planes. All common mesh details and the first mesh level are shown in **Figure 11a**.

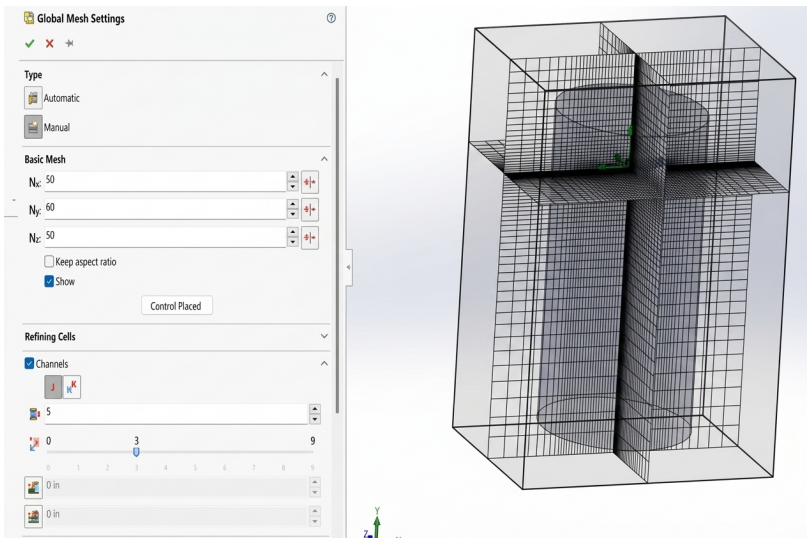

(a)

Figure 11. *Cont.*

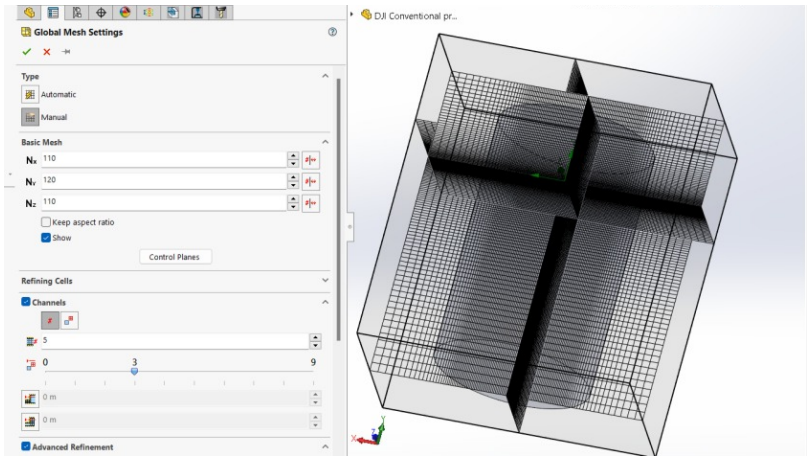

(b)

Figure 11. Mesh iterations, **(a)** First iteration; **(b)** Selected mesh.

The graph in **Figure 12** shows the result of the thrust after each iteration, and the mesh level represents an increment of 10 on all axes for each level. From this graph, it is clear that at the 7th and 8th level the results started to converge and looking at the value, it indicated a convergence towards the actual value of 9.8 N. However, this also happened at the 3rd and 4th level, therefore it is not possible to base the choice only on this convergence, because looking at the first equal double value, the values differed a lot when the mesh increased. In addition to the thrust value, further analysis of the plots of the noise emitted indicates that the result really started to converge.

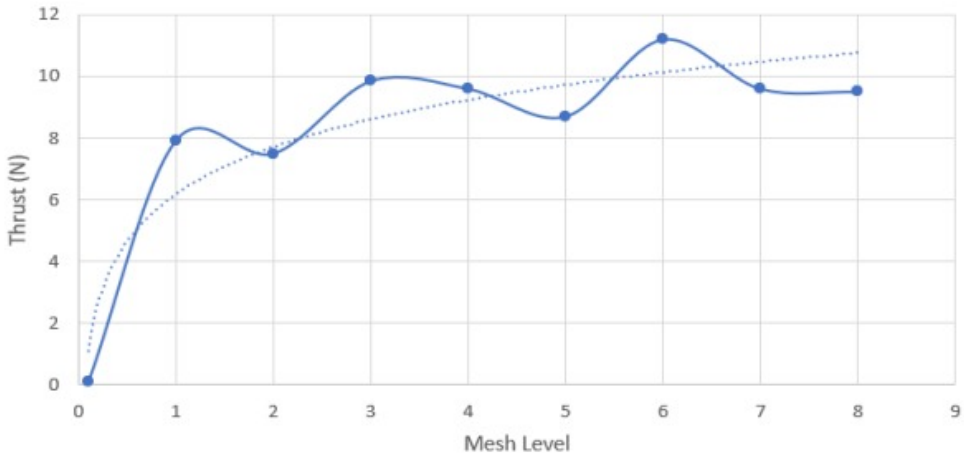

Figure 12. Plot of the mesh independency curve.

Examining **Figure 13a,b**, they are extremely similar where no visible changes are detectable, as for **Figure 13c,d**, it is clear that the plots were still drastically changing with a finer mesh. Level 7 and level 8 gave both the same thrust value of around 9.6 N having as a relative error of around 2.34%. Therefore, in conjunction with the cut plot analysis mentioned previously, the selection of a mesh with level 7 shown in **Figure 11b** was selected for the whole study since it gave the same results as the level 8th with much less simulation time, making it more efficient especially for a parametric study.

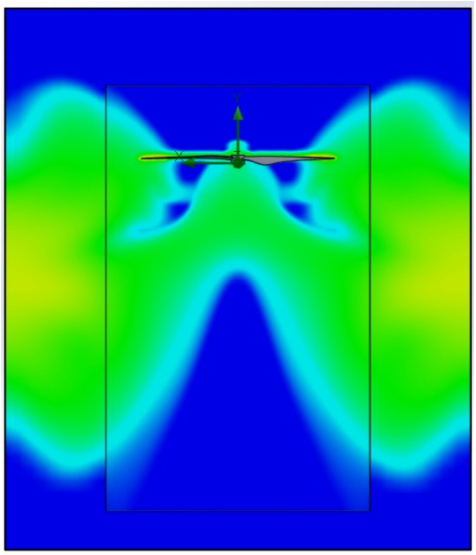

(a)

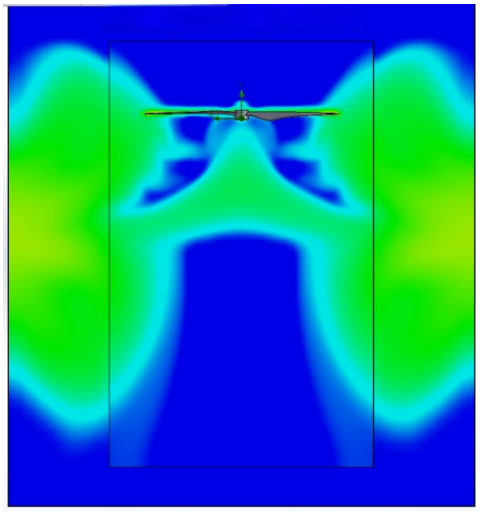

(b)

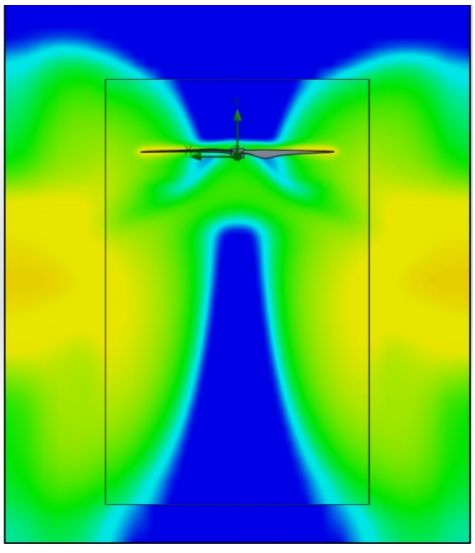

(c)

Figure 13. *Cont.*

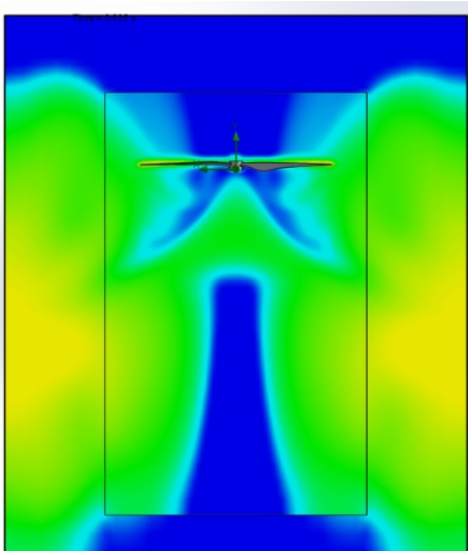

(d)

Figure 13. Noise level emitted cut plots for different mesh levels, **(a)** Mesh level 7; **(b)** Mesh level 8; **(c)** Mesh level 3; **(d)** Mesh level 4.

2.3. Experimental setup

To validate the numerical results, an experimental study was conducted that included thrust and dB measurements for different values of RPM for both the oval toroidal and the conventional propeller (**Figure 14**).

Figure 14. Experimental set up.

The selection of the oval instead of the circular was mainly based on the fact that the oval represented better performance according to the simulations done in the previous part. In addition to that, some structural concerns had to be taken into consideration, where the circular one had no resistance to the structural stresses that were posed on it when the motor was turned on, basically the blade broke and was not able to withstand the centrifugal force. For future usages, this can be fixed by either changing the thickness of the blade, which would also interfere in its aerodynamic performance, that was the reason why it was not changed, or by either changing the material and choosing one that can handle these stresses.

The apparatus of this experiment included a balance that was used to measure the thrust and a tachometer to measure the different RPM at different throttle settings. The

experiment went as follows: First the preparation of the drone and the scale was made, the rectangular wooden piece was added to be able to place the drone and distribute the load uniformly on the scale that had a small surface. During the experiment, only two propellers were attached to reduce the overall generated thrust to be able to increase the RPM and get more experimental value before the drone "takes off" the scale. Aluminum tape was added to the blade of the propeller in order for the tachometer to catch the rotation and give accurate measurements of the RPM.

The scale was set to zero when the motors were off, then when the motors were switched on, the negative reading indicated the generated thrust. The motor throttle then increased progressively 5% and for each setting, thrust measurements were taken starting at idle with an opening of 10%. The same process was repeated for both conventional and oval toroidals.

3. Results

3.1. Circular toroidal results

The main parameters that were monitored in this parametric study were the thrust and acoustic power generated by the propellers. However, it is also important to monitor changes in air resistance, as this factor significantly impacts motor performance. An increase in air resistance can reduce the actual rotational speed of the propeller compared to the ideal speed set by the throttle. It is important to keep track of this parameter in order to know when it is needed and when the designed propellers become unfeasible due to very high stresses on the blades, from a structural point of view, and stresses on the motor itself, which will shorten its life span.

From all the cut plots showing the noise emission distribution in **Figure 15**, a pattern can be visualized that shows the variation of the flow distribution and the generation of vortices that result mainly in high noise emission. In **Figure 15a** and **Figure 15b**, lower intensity vortices are generated, which was expected to have a lower normal area facing the airflow, decreasing the flow separation.

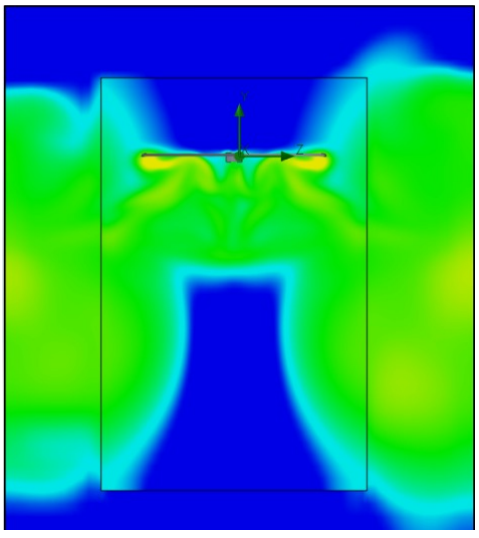

(a)

Figure 15. *Cont.*

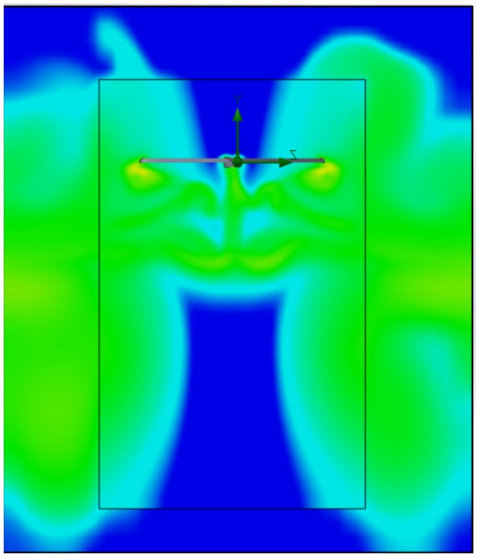

(b)

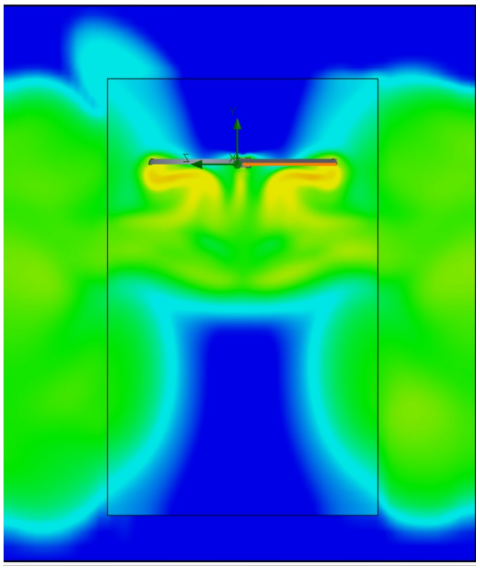

(c)

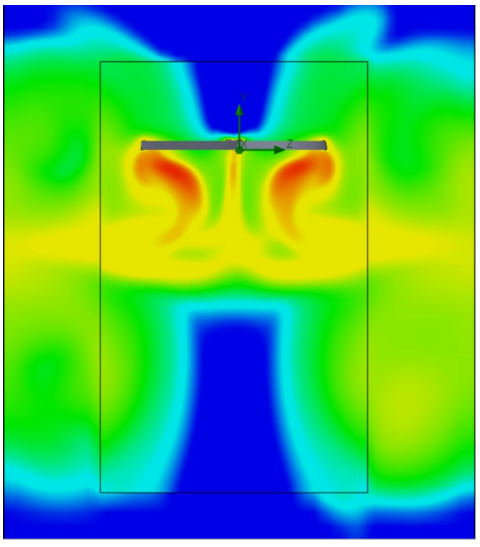

(d)

Figure 15. *Cont.*

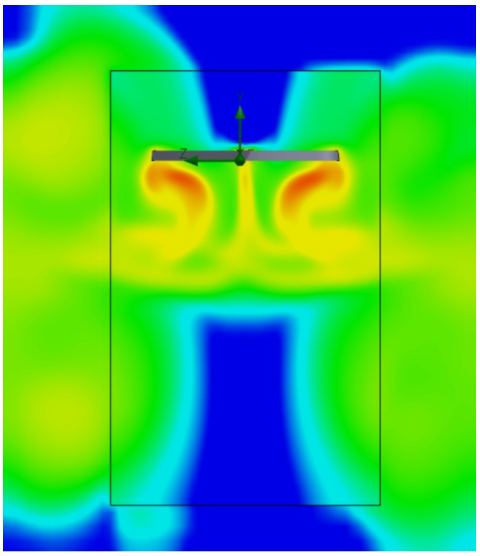

(e)

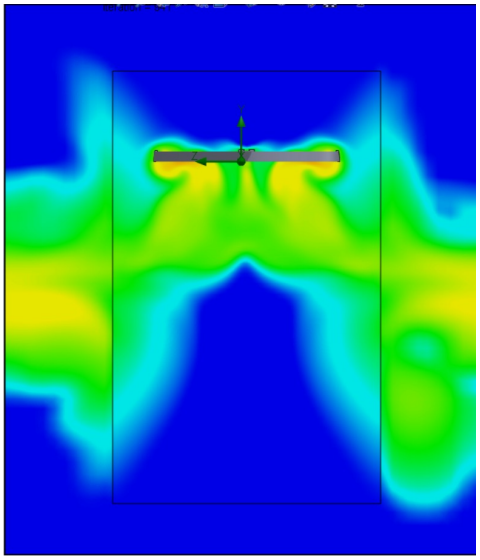

(f)

Figure 15. Noise level cut plots for for different pitch angles for the circular toroidal, **(a)** 10°; **(b)** 15°; **(c)** 20°; **(d)** 35°; **(e)** 40°; **(f)** 45°.

Starting from the angle 20°, a similar pattern appeared with stronger vortices, and as seen in **Figure 15d** continued to increase with increasing pitch angle. These results were consistent with the results obtained and shown in **Figure 16b**, where an increase in angle also showed an increase in noise generation, with some local exception due to some particular aspects. In addition, they showed consistency with the research previously mentioned that the main noise comes from the tip of the blades, where it is clear that the intense vortices start from the tip, highlighting the importance of the toroidal shaped propellers.

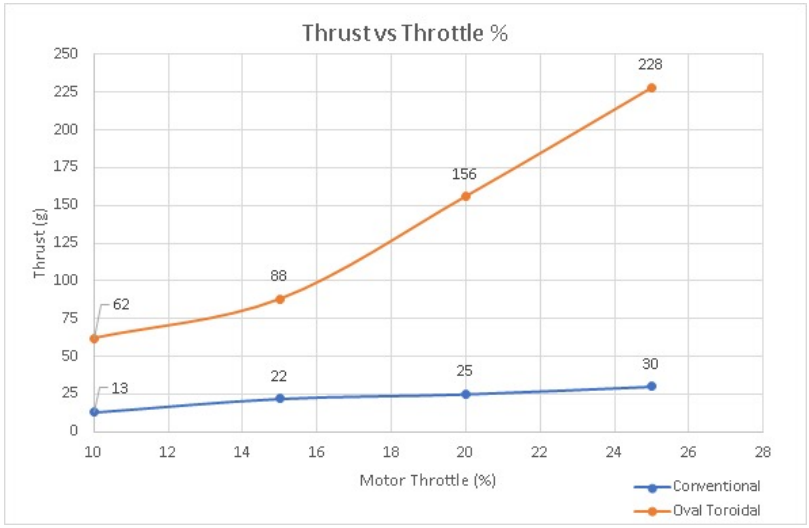

(a)

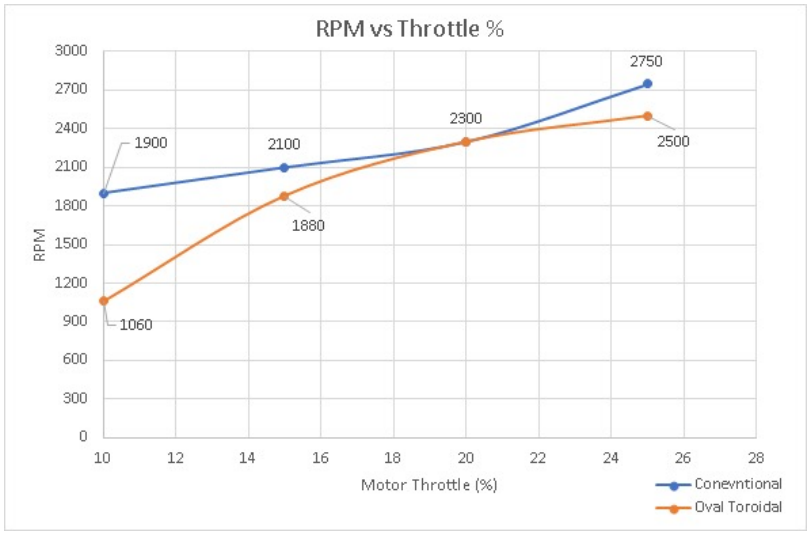

(b)

Figure 16. Plots of the experimental results with respect to motor throttle, **(a)** Thrust; **(b)** RPM.

An interesting aspect appeared also for the plot of the simulation at a pitch angle of 45°, where the airflow particles started to shift more and more sideways instead of remaining directly beneath the propeller as shown in **Figure 15f**. This could be due to the way the blades strike the airflow when having such high pitch angles. This analysis can be backed up by examining **Figure 17** where it is apparent that at high angles of attack the flow separation occurs near the leading edge which leads to a separation that tends to occur more at a higher location than the airfoil itself [21], which in the case of the rotating propeller this would translate into a radial propagation of the vortices, and not directly beneath the blades.

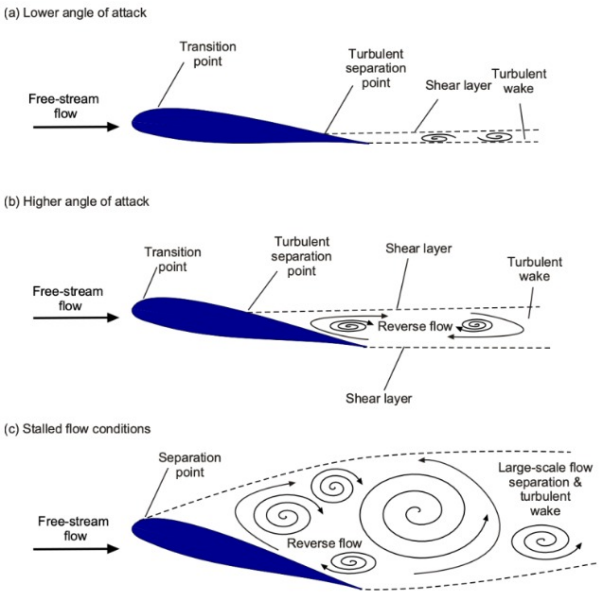

Figure 17. Airflow behavior at high angles of attack [5].

The cut plots shown in **Figure 18a,b**, show a projection of the noise distribution from the top view located at a distance of 25 cm underneath the propeller. The maximum value of these plots was the values registered in the plots shown in the discussion in **Figure 19b**. It is important to note that by looking only at that plane, no accurate conclusions can be drawn, and it is not possible to evaluate the absolute general behavior and performance of the propeller.

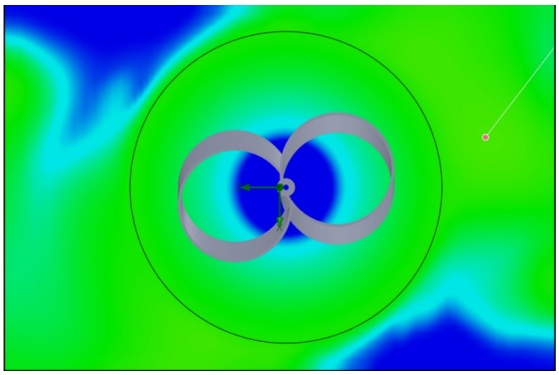

(a)

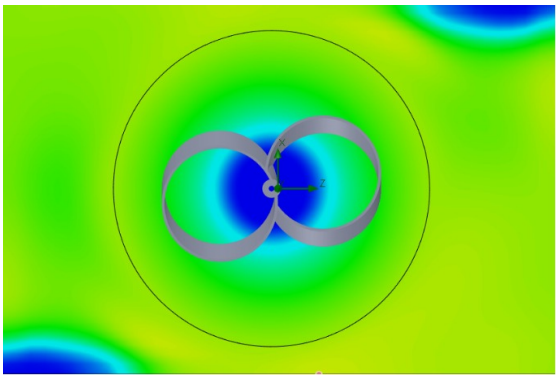

(b)

Figure 18. Noise level cut plots for different pitch angles for the circular toroidal, **(a)** 15°; **(b)** 35°.

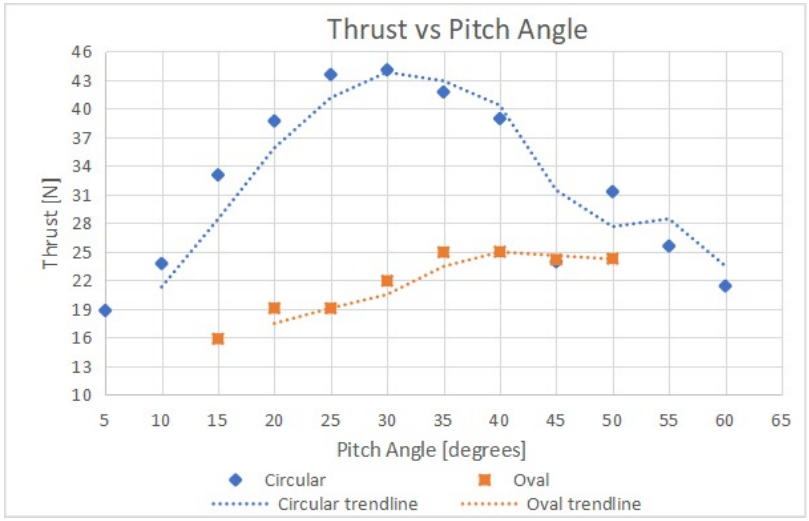

(a)

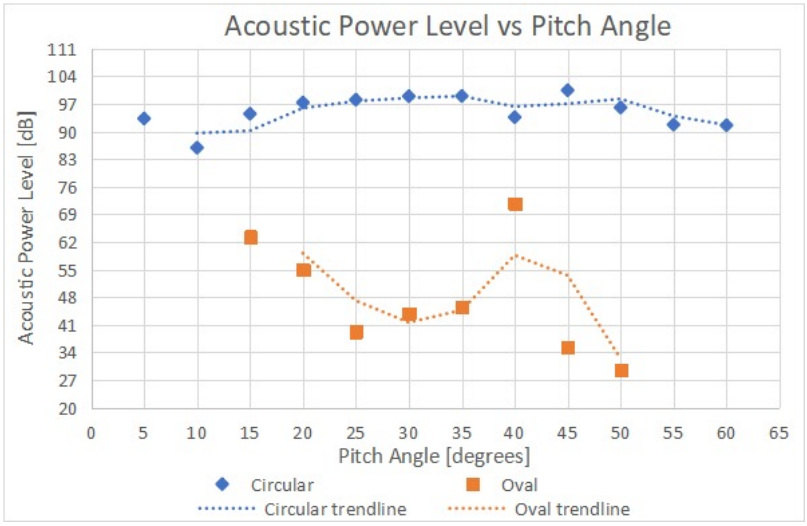

(b)

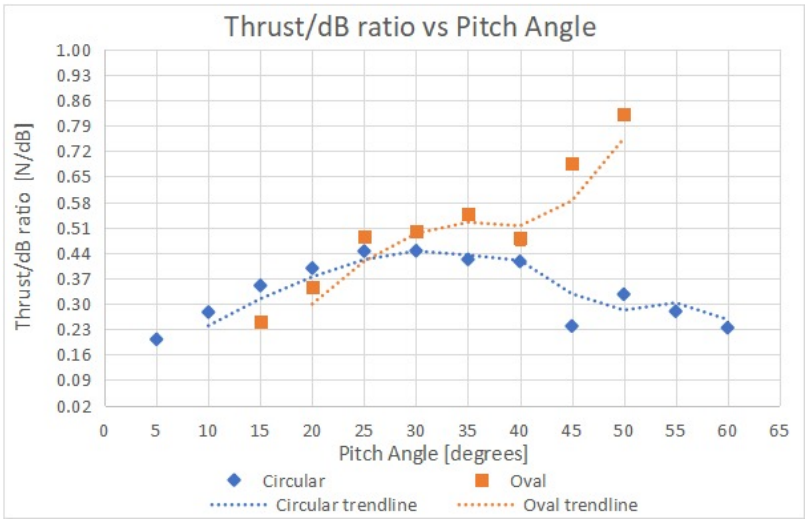

(c)

Figure 19. *Cont.*

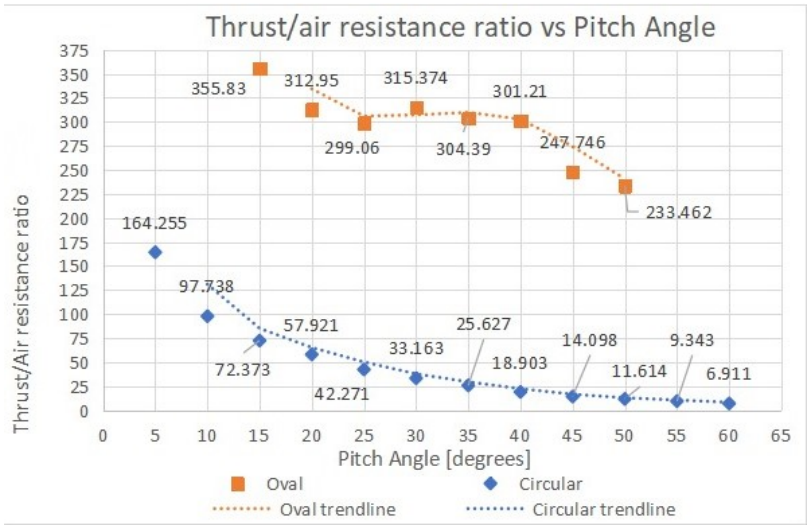

(d)

Figure 19. Plots of the results for the oval toroidal propeller with respect to pitch angle, **(a)** Thrust; **(b)** Noise power level; **(c)** Thrust/dB ratio; **(d)** Thrust/drag ratio.

However, they still show somewhat a very close behavior to the reality where almost all of the iterations had a consistent interpretation by looking at the cut plot that shows the whole distribution from the front view and the one that is 25 cm beneath the blade.

For example, from the front view projection, it is possible to interpret that the blade at an angle of 35° produces more noise than the one at an angle of 15°, since much more intense vortices appear, indicated by the red and yellow colors in the plot. The same conclusion can be made from the top view projections, where the yellow color can also be seen as more dominant, which was also the result obtained from the graphs.

The same analogy was made for the other graphs and all values showed the same consistency, only in the case of the pitch angle of 45°, the cut graphs did not show the same conclusion and kind of contradicted each other, where in the front view no extreme noise generation can be observed, however, with respect to the maximum value, it showed a higher value.

To conclude the graphs interpretation, it is important to also look at the cut plots and the overall behavior of the airflow over the whole domain. In the end if one vortex appeared in that plane, a higher maximum value would be taken, marking that at this certain pitch angle a higher noise was emitted, but when the whole cut plot is analyzed, it could be the case that the blue and green colors are much more dominant in that corresponding plot, indicating an overall lower value for the noise generated, marking a huge contradiction. All cases have been studied, and the analysis was performed for both cut plots and no contradiction was found in around 90% of the results.

3.2. Oval toroidal results

The same cut plots were implemented in the oval toroidal simulations and had the same motivation. However, for this propeller there was no pattern followed by airflow at certain angle values as was the case for the circular toroidal one, except for the last two values which are 40° and 45°, which are almost exactly the same. As in the other

plots shown, each angle has its own airflow distribution.

This strange and unpredictable behavior had a huge effect on the projection in the cut plots shown in **Figure 20a,b** and the results obtained in the graphs in **Figure 19b**.

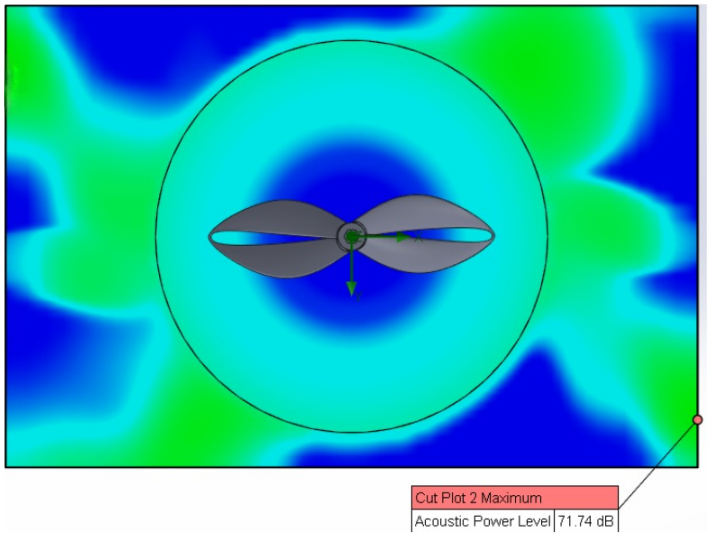

(a)

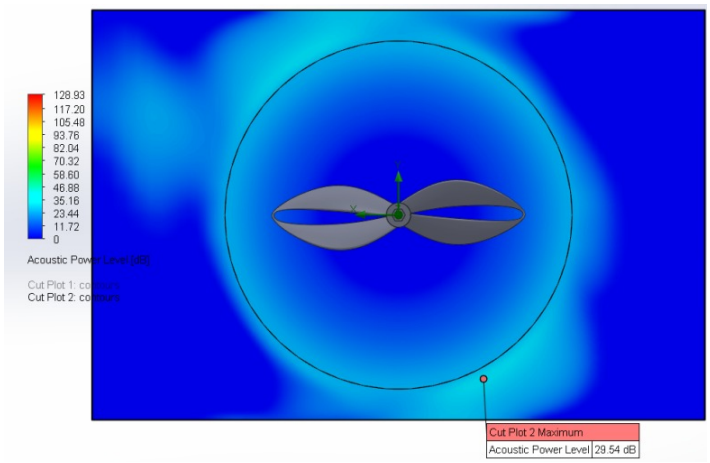

(b)

Figure 20. Noise level cut plots for different pitch angles for the oval toroidal, **(a)** 35°; **(b)** 45°.

The fact that the airflow distribution especially for the highest pitch angles resulted in a projection on the 25 cm distanced plane from the top view that is mainly dominated by lower values, as can be easily observed in the plot of 45°. These results can be more misleading than the ones already mentioned and talked about for the circular toroidal, therefore; a deeper analysis similar to the one mentioned above was conducted. However, although no final accurate values can be computed, however; the overall behavior remains reliable and consistent.

A comparable trend is observed for both oval and circular toroidal propellers, where the most intense vortical structures consistently form at the blade tips, further underscoring the relevance of toroidal geometries. In addition, increasing the pitch angle leads to the development of stronger vortices, a result that may initially appear counterintuitive when considered in terms of the thrust-to-noise ratio. This apparent contradiction is explained by the spatial distribution of noise intensity. Although higher

pitch angles generate more intense vortices, the overall area occupied by high-intensity regions (green and yellow) in **Figure 21e** is considerably smaller than that observed in **Figure 21b**. When this spatial distribution is taken into account, the results remain fully consistent.

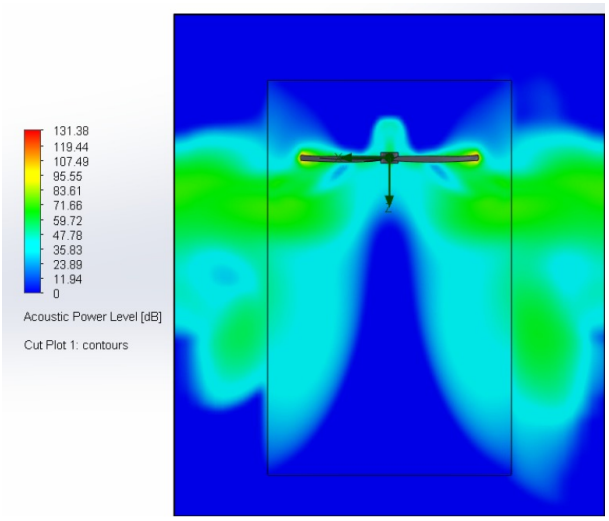

(a)

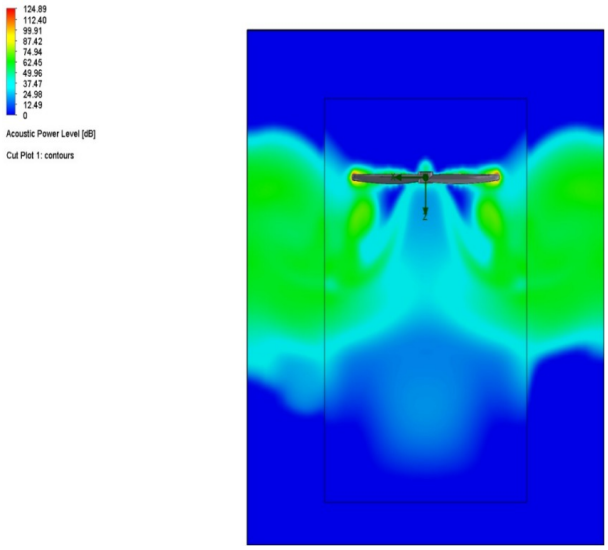

(b)

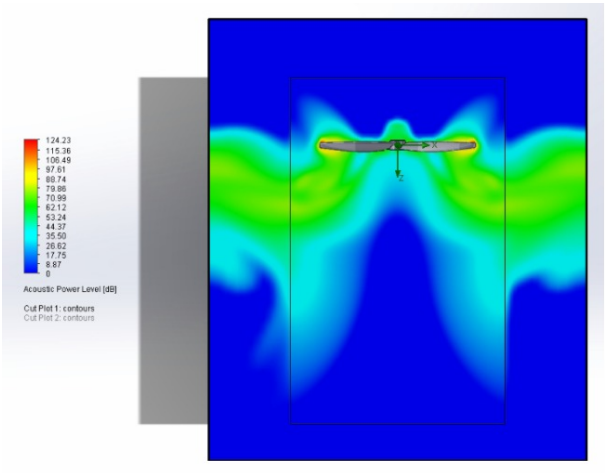

(c)

Figure 21. *Cont.*

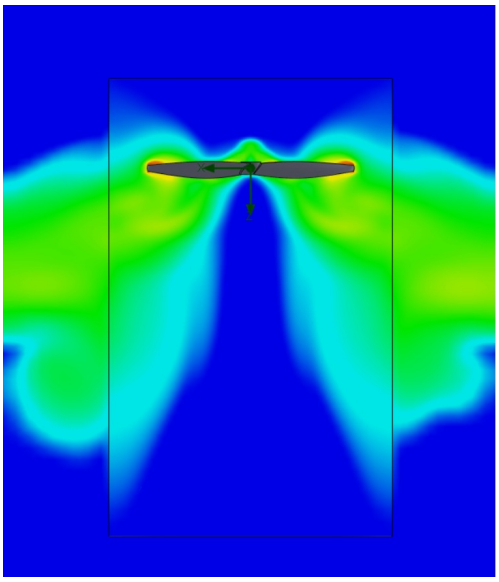

(d)

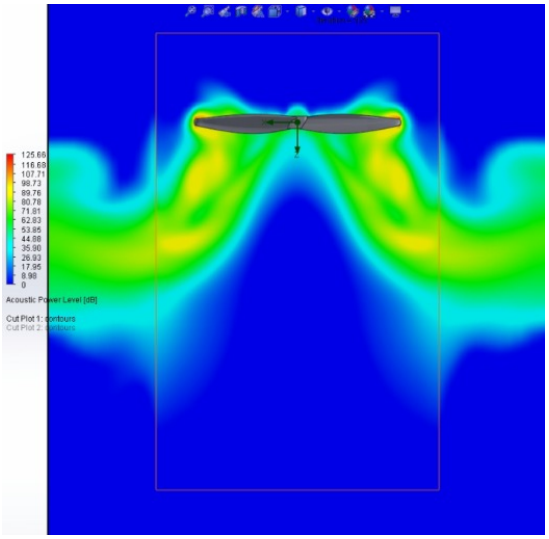

(e)

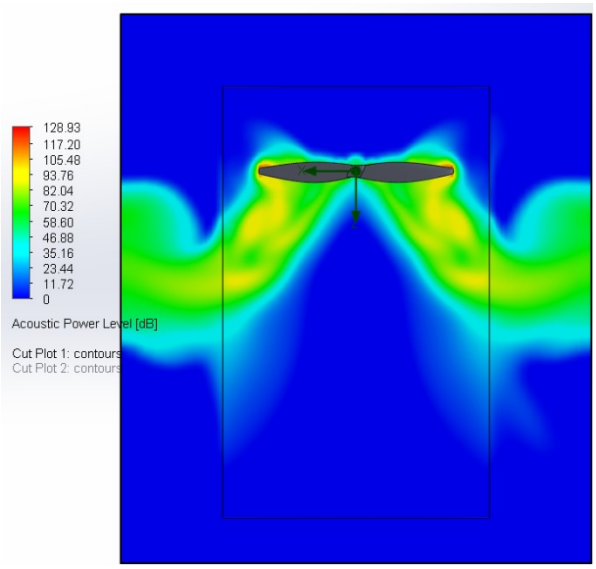

(f)

Figure 21. Noise level cut plots for different pitch angles for the oval toroidal, **(a)** 10°; **(b)** 20°; **(c)** 25°; **(d)** 35°; **(e)** 40°; **(f)** 45°.

An illustrative analogy can be drawn with a sine wave of high amplitude evaluated over a single period, which yields a smaller enclosed area than a lower-amplitude wave evaluated over multiple periods; a similar interpretation applies in the present case. This behavior is closely related to blade geometry, as the circular toroidal propeller incorporates an airfoil profile optimized for drag control and vortex generation, in contrast to the comparatively flatter blade geometry of the oval configuration. This observation highlights an additional key parameter for future investigations, namely the influence of blade airfoil design on both aerodynamic and acoustic performance.

Finally, a marked distinction between the oval and circular toroidal propellers is evident in the front-view cut plots. The absence of red-colored vortices in the oval configuration indicates substantially weaker vortex formation compared to the circular design. This outcome is consistent with expectations, given the differences in airfoil geometry and their respective interactions with the surrounding flow.

4. Discussion

This section presents a detailed discussion and interpretation of the results obtained from both the parametric numerical simulations and the experimental measurements, with particular emphasis on comparing the performance of the different propeller configurations. For the circular toroidal propeller, a clear trend is observed in **Figure 19a,b**, where an increase in generated thrust is generally associated with a corresponding rise in acoustic power. An exception to this behavior occurs at a pitch angle of 10°, where a noticeable reduction in acoustic power is observed despite an increase in thrust. This deviation indicates that parameters other than pitch angle alone, such as flow separation and the spatial distribution of vortical structures, play an important role in the noise generation process.

For the oval toroidal propeller, the thrust variation presented in **Figure 19a** follows the expected trend, increasing with pitch angle up to 35°, beyond which it remains nearly constant. The most pronounced change at higher pitch angles is observed in the acoustic response, as shown in **Figure 19b**, where a sharp decrease in acoustic power occurs, reaching a minimum value of 29.54 dB. This behavior suggests that while thrust production stabilizes at elevated pitch angles, noise emission is significantly reduced, highlighting a potential advantage of the oval toroidal configuration in achieving a favorable compromise between aerodynamic performance and acoustic efficiency.

Figure 19c,d illustrate the thrust-to-acoustic power ratio and the thrust-to-drag ratio, respectively, which provide insight into the relative variation of these performance metrics. Higher values of these ratios are desirable, as they correspond either to configurations that produce substantial thrust with comparatively low noise emission or to propellers that achieve high thrust levels overall. Consequently, the selection of an optimal propeller design requires balancing these ratios against the absolute thrust generated. Similarly, a high thrust-to-drag ratio indicates that aerodynamic resistance remains relatively low at the corresponding pitch angle. This parameter is particularly useful for defining design limits prior to fabrication, as configurations falling below a prescribed threshold may be considered unsuitable for practical applications.

4.1. Analysis of simulation outcomes

An examination of the curves presented in **Figure 19a** indicates that the circular toroidal propeller generates the highest thrust levels, ranging from a minimum of 18.84 N at a pitch angle of 5° to a maximum of 44.08 N at 30°. By comparison, the oval toroidal propeller produces a minimum thrust of 15.87 N at 15° and reaches a peak value of approximately 25 N at 40°. The overall trends exhibited by the two profiles differ markedly. The circular configuration shows a steep increase in thrust, starting from relatively low values, rising rapidly to a maximum, followed by a sudden drop and a continued decline beyond 50° as the pitch angle increases. In contrast, the oval configuration displays a more stable behavior, characterized by moderate incremental increases and an almost constant thrust level of about 24.5 N between 35° and 50°.

At first glance, the higher thrust generated by the circular profile may appear counterintuitive, since airfoils with greater camber and thickness are generally associated with higher lift generation [9]. However, the circular blade can be approximated as an inclined flat plate with limited camber and reduced thickness relative to the oval profile. A plausible explanation for its superior thrust performance lies in the larger blade surface area of the circular design, as illustrated in **Figure 2a** and **Figures 4a**. Further refinement and optimization of the oval airfoil geometry could therefore lead to improved thrust performance in future investigations.

Most notably, both toroidal propeller configurations demonstrate the capability to generate substantially higher thrust than the conventional propeller. This result is expected, as the toroidal architecture incorporates four rotating blades rather than two, leading to an inherent increase in thrust production. The second set of results, presented in **Figure 19b**, addresses the acoustic performance of the investigated designs. In contrast to the thrust behavior, the oval toroidal propeller exhibits more favorable noise characteristics than the circular configuration. The oval design reaches a maximum acoustic power of 71.74 dB at a pitch angle of 40°, while the minimum value, 29.54 dB, is recorded at 50°, measured on a plane located 25 cm below the propeller.

By comparison, the circular toroidal propeller produces consistently higher noise levels than both the oval toroidal and the conventional propellers, with a maximum acoustic power of 100.44 dB at 45° and a minimum of 85.88 dB at 10°. This elevated acoustic response is likely associated with the high thrust levels generated by the circular design, as the data clearly indicate a correlation between thrust production and noise emission. In addition, the circular blade geometry, which can be approximated as an inclined flat plate, promotes increased wake turbulence [22], thereby intensifying noise generation [11]. This behavior is clearly illustrated in **Figure 15d,e**, where the vortex structures exhibit markedly higher intensity.

An additional observation relates to the spatial distribution of airflow and the resulting noise patterns. As shown in **Figure 15e,f**, the maximum acoustic power occurs at a pitch angle of 45°, yet the corresponding cut plots indicate that at 40°, despite a lower recorded noise level, the vortices appear more intense, as evidenced by the red regions. Similarly, **Figure 15d** at 35° displays even stronger vortical structures than those at 40°, while still yielding a lower acoustic power level. These results suggest that vortex intensity alone does not directly dictate noise emission. A comparable trend

is observed for the oval toroidal propeller. In **Figure 21e**, the relatively low acoustic power measured 25 cm below the propeller is attributed to the lateral deflection of the airflow, in contrast to **Figure 21a**, where vortices are more broadly distributed. Consequently, definitive conclusions cannot be drawn from a single measurement plane. A more comprehensive assessment should therefore consider the total radiated noise across multiple planes, as localized high-intensity vortices, such as those observed in **Figure 21e**, may coexist with lower overall acoustic emissions, whereas broader vortex distributions, as in **Figure 21a**, may contribute more significantly to global noise levels.

Evaluating propeller performance solely on the basis of thrust and acoustic power is insufficient, particularly given that the circular configuration demonstrates superior thrust generation, whereas the oval configuration exhibits enhanced noise reduction. A more representative performance indicator is the thrust-to-acoustic power ratio, as it simultaneously accounts for both parameters. It is worth noting that the pitch angle corresponding to maximum thrust does not coincide with the angle yielding minimum noise emission. As shown in **Figure 19c**, the circular toroidal propeller attains its lowest thrust-to-dB ratio at a pitch angle of 60° (0.234), indicating poor operational efficiency under these conditions. Its highest ratio is observed at 30°, reaching a value of 0.445, which corresponds to a thrust of 44.08 N and an acoustic power of 98.94 dB.

In contrast, the oval toroidal propeller achieves a substantially higher peak ratio of 0.822 at 50°, while generating only 29.54 dB of noise and producing 24.28 N of thrust. Even when this extreme case is excluded, the oval configuration maintains superior performance. At a pitch angle of 35°, it records a thrust-to-dB ratio of 0.548, corresponding to 24.96 N of thrust and 45.51 dB of acoustic power, thereby outperforming the circular design. For reference, the conventional propeller exhibits a considerably lower ratio of 0.126, producing 8.83 N of thrust and emitting 73.21 dB of noise, which is significantly inferior to both toroidal configurations under their respective optimal operating conditions.

Figure 19d presents the variation of aerodynamic resistance across the investigated pitch angles. This parameter is of particular importance, as it reflects real operating conditions in which drag directly affects motor efficiency and leads to a reduction in achievable rotational speed. The results indicate that the oval toroidal propeller experiences substantially lower aerodynamic resistance than the circular configuration, an outcome that is consistent with the circular blade's resemblance to an inclined flat plate. At a pitch angle of 40°, the circular propeller exhibits an exceptionally high drag ratio of 18.903, rendering it impractical for real-world applications. Although slightly lower values are observed at higher pitch angles, the drag levels remain unfavorable.

4.2. Analysis of experimental outcomes

The experimental results are shown in **Figure 16**, where the variation of the thrust is shown with respect to the throttle. It is obvious that the thrust in toroidal is much higher than the one generated by conventional, where it is almost 4 times higher. As for **Figure 16b**, it represents the variation in the RPM where the toroidal had a lower RPM at the same throttle setting, which indicates that the toroidal led to a decrease in

motor efficiency. The results showed the effectiveness of the toroidal propellers when it comes to increasing the thrust, as for the noise emitted, the results of the experiment showed a reduction of approximately only 10 db.

The reason behind this difference between the experimental and real values came from the roughness of the propeller surface, first because of the manufacturing, which is very visible with the naked eye and second because of the added tapes already mentioned for better tachometer functionality and the ones that were also added to balance the propeller as shown in **Figure 22**. The rough surfaces of the propeller greatly increase turbulence and flow separation [5], which in turn increases the emitted noise [23]. Finally, the noise test was not performed in a well-equipped studio, which would also increase the chances of errors. However, with all that extra drag and the decrease in the RPM of the motor, the toroidal also showed better performance for both thrust and noise reduction.

Figure 22. Surface roughness of the manufactured blades.

5. Conclusion

In this paper, computational simulation and modeling alongside experimental results were studied to see the effect of the geometry of a propeller on the thrust and noise level generated. It was shown that, when thrust and the level of acoustic power are taken into account, the most optimal configuration for the circular toroidal was at 30°; also at this angle the thrust-to-air resistance ratio is acceptable, making this propeller functional also in real life applications. The best configuration for the oval is the [40°, 35°], with the first angle being the one at the base [24].

Comparing all three together, with each at its most optimum configuration, they rank from the best to the worst, the oval toroidal, the circular toroidal, and finally the conventional one.

Finally, it is not possible to just select one that is the most optimum for all cases, it is possible to have different configurations that do not have the highest N/dB ratio, or even the circular could be preferred over the oval in some cases depending on what is requested from the mission. Therefore, there should be a trade-off between noise and thrust, and each parameter, depending on the mission, should have a weighing factor that marks which is more desirable [25].

To enhance the rigor of this approach, the Combined Performance Score (c) is derived from a Multi-Objective Optimization (MOO) framework:

1. Metric Identification: We utilize the Thrust-to-Acoustic Power Ratio (N/dB) as the primary indicator of efficiency.
2. Boundary Conditions: We define x as the N/dB ratio at maximum thrust and y as the ratio at minimum noise.
3. Linear Scalarization: We introduce weighting factors α (thrust priority) and λ (noise priority), where $\alpha + \lambda = 1$.
4. Equation Derivation: By interpolating between boundary states, we establish the scoring function: $c = \alpha x + \lambda y$.

The following method would help to select the appropriate propeller, with the appropriate configuration according to the mission, and the steps are as follows:

1. Assign weighting factors: select the weighing factors α (for thrust) and λ (for noise) according to mission priorities.
2. Identify key angles: for each propeller type, determine the pitch angle that yields the highest thrust and the angle with the lowest noise level.
3. Calculate Thrust-to-dB ratios for each selected angle.
4. Apply the combined performance equation: replace the ratio corresponding to maximum thrust with x, and the ratio for minimum noise with y, then compute the value the combined performance score c from the below equation:
$$c = \alpha x + \lambda y$$
5. Match the score to the closest angle: compare the calculated c value to the ratios across all angles and identify the closest match for both circular and oval propellers.
6. Select the optimal configuration: review the thrust and noise values for the chosen angles and select the propeller type that best satisfies the mission criteria.

Assume for example, $\alpha = 0.7$ (thrust priority) and $\lambda = 0.3$ (noise priority), with the summation always equal to 1.

For the oval propeller:

- Highest thrust occurs at 40°, with a thrust-to-dB ratio of 0.348.
- Lowest noise occurs at 50°, with a ratio of 0.828.
- Applying the formula:
$$c = \alpha x + \lambda y = 0.7 \times 0.348 + 0.3 \times 0.828 = 0.492$$

From **Figure 19c**, this combined ratio corresponds to an angle between 45° and 50°, closer to 45°, making this the best oval configuration for the selected weighting factors. For more precision, linear interpolation can be applied since variations between iterations are small.

For the circular propeller, applying the same steps gives an optimal angle of 15°, where:

- Thrust = 33.06 N
- Acoustic power = 94.48 dB

For comparison, the oval toroidal propeller operating at a pitch angle of 45° delivers a thrust of 24.18 N while emitting 35.24 dB of noise. Based on the selected

weighting factors, the optimal configuration for this specific case corresponds to the circular toroidal propeller at 15°. However, when the relatively modest difference in thrust is weighed against the substantial reduction in noise, the oval configuration operating at 50° or 45° may be favored in applications where acoustic constraints are critical [26]. Finally, the thrust-to-drag ratio should also be evaluated, particularly for long-duration missions, as excessive aerodynamic resistance can significantly reduce overall efficiency and compromise operational feasibility.

Table 1 presents suggested weighting factors for various mission types, along with descriptions and the rationale behind each selection. These factors are not fixed and may be adjusted if the mission's objectives differ from the cases outlined in the table. The purpose of this table is to provide clearer guidance on how to choose and prioritize these factors based on specific operational requirements.

Table 1. Suggested weighing factors for different mission types.

Mission	Description	Motive	α	λ
Search & rescue	Any emergency case, looking in the aftermath of a natural disaster, lost person in a remote hard to reach area. Could also include a delivery of emergency supplies such as first aid kit.	The main focus is on saving the person, the main concern should be high thrust to consume less power and have more endurance, noise shouldn't be a concern.	0.9	0.1
Delivery (day time, city)	Any package delivery, where the main location of the mission is located in a crowded city and during the day time.	In a crowded area during day time where it will mostly be noisy, the drone noise impact will be minimal.	0.4	0.6
Delivery (night time, city)	Any package delivery, where the main location of the mission is located in a crowded city and during the night time.	Without the noisy environment of the city, the impact of the noise emitted by the drone will increase.	0.3	0.7
Delivery (day time, suburbs)	Any package delivery, where the main location of the mission is located in a calm and not a noisy area during the day time.	For a suburb area, even during the day the area is generally not that noisy so the drone will have an impact and will be relatively noisy.	0.3	0.7
Delivery (night time, suburbs)	Any package delivery, where the main location of the mission is located in a calm and not a noisy area during the night time.	During the night, the drone's noise will most likely be dominant. If changed the thrust shall not be higher than 0.2	0.1	0.9
Photography	Any photography used for all purposes, whether a marriage, an event or a movie. Weighing factors could differ if the photography was for natural wild life.	Any photography for an event or a movie, the noise might appear in the video. In case of a wildlife tracking or photography, the noise shall be much more favored.	0.4/0.2	0.6/0.8
Construction services	Sky scrapers window cleaning, monitoring, maintenance, painting.	For this case, mission will usually in the day, crowded area and the sky scraper will most likely equipped with noise proof windows, noise have little impact.	0.7	0.3
Mapping	Geographical mapping, used to create 2D maps or even 3D maps, any service related to any landscape observation. Weighing factors could differ in case of mapping in an area with wildlife.	In case of performing the mission during the day in a city, thrust can have a higher factor. In the case of mapping a place where wild life shall be considered than the noise shall have a really high importance.	0.4/0.2	0.6/0.8
Agriculture services	Services related to monitor or check on plants in farms, water spraying or anti pesticide spraying.	These services will mainly be achieved in areas where there are no people. High thrust shall be favored.	0.8	0.2

Author contributions: Conceptualization, RN, MS EAJ, CA, and JR; methodology, JR; software, RN, MS, EAJ, and CA; validation, JR; formal analysis, RN, MS, EAJ, and CA; investigation, RN, MS, EAJ, and CA; resources, JR; data curation, RN, MS, EAJ, and CA; writing—original draft preparation, RN and JR; writing—review and editing, JR; visualization, RN, MS, EAJ, and CA; supervision, JR; project administration, JR. All authors have read and agreed to the published version of the manuscript.

Funding: This research did not receive any specific grant from funding agencies in the public, commercial, or not-for-profit sectors.

Institutional review board statement: Not applicable.

Informed consent statement: Not applicable.

Data availability statement: The data used to support the findings of this study are available from the corresponding author upon request.

Conflict of interest: The authors declare no conflict of interest.

References

1. A brief history of drones: From pilotless balloons to roaming killers. Available online: https://interestingengineering.com/innovation/a-brief-history-of-drones-the-remote-controlled-unmanned-aerial-vehicles-uavs (accessed on 5 October 2025).
2. Schäffer B, Pieren R, Heutschi K, et al. Drone Noise Emission Characteristics and Noise Effects on Humans—A Systematic Review. International Journal of Environmental Research and Public Health. 2021; 18(11): 5940. doi: 10.3390/ijerph18115940
3. Christian AW, Cabell R. Initial Investigation into the Psychoacoustic Properties of Small Unmanned Aerial System Noise. In: Proceedings of the 23rd AIAA/CEAS Aeroacoustics Conference; 5–9 June 2017; Denver, CO, USA. doi: 10.2514/6.2017-4051
4. McKay RS, Kingan MJ, Go ST, et al. Experimental and analytical investigation of contra-rotating multi-rotor UAV propeller noise. Applied Acoustics. 2021; 177: 107850. doi: 10.1016/j.apacoust.2020.107850
5. Sebastian T, Strem C. Toroidal Propeller. US20190135410A1, 17 November 2020. Available online: https://patents.google.com/patent/US20190135410A1/en
6. Ghoreyshi M, Aref P, Wisniewski CF, et al. Computational investigation of quiet propeller designs for small unmanned aerial vehicles. Aerospace Science and Technology. 2023; 138: 108351. doi: 10.1016/j.ast.2023.108351
7. Wang Chunhui, Liu S, Xia K, et al. Numerical research on hydrodynamic performance of toroidal propeller under the influence of geometric parameters. Ocean Engineering. 2024; 314: 119704. doi: 10.1016/j.oceaneng.2024.119704
8. DJI Innovations. DJI F450 User Manual v2.2. DJI Innovations; 2013.
9. Prajapati R, Kumar BP, Kushwaha S, et al. Comparing Toroidal Propeller Performance with Different Blade Numbers at Different RPM: CFD Analysis and Evaluation. International Journal of Engineering Research & Technology. 2024; 13(4). doi: 10.5281/ZENODO.18145166
10. Kawai C, Jäggi J, Georgiou F, et al. Short-term noise annoyance towards drones and other transportation noise sources: A laboratory study. The Journal of the Acoustical Society of America. 2024; 156(4): 2578–2595. doi: 10.1121/10.0032386
11. Green N, Torija AJ, Ramos-Romero C. Perception of noise from unmanned aircraft systems: Efficacy of metrics for indoor and outdoor listener positions. The Journal of the Acoustical Society of America. 2024; 155(2): 915–929. doi: 10.1121/10.0024522
12. König R, Babetto L, Gerlach A, et al. Prediction of perceived annoyance caused by an electric drone noise through its technical, operational, and psychoacoustic parameters. The Journal of the Acoustical Society of America. 2024; 156(3): 1929–1941. doi: 10.1121/10.0028514
13. Lotinga MJB, Green MC, Torija AJ. Human perception and response to sound from unmanned aircraft systems within ambient acoustic environments. Npj Acoustics. 2025; 1(1): 2. doi: 10.1038/s44384-024-00001-6
14. Yang C, Wallace RJ, Huang C. A Review and Bibliometric Analysis of Unmanned Aerial System (UAS) Noise Studies between 2015 and 2024. Acoustics. 2024; 6(4): 997–1020. doi: 10.3390/acoustics6040055
15. Hua J, Mankbadi RR. Prediction and Control of Broadband Noise Associated with Advanced Air Mobility—A Review. Applied Sciences. 2024; 14(18): 8455. doi: 10.3390/app14188455
16. Raza W, Stansbury RS. Noise Prediction and Mitigation for UAS and eVTOL Aircraft: A Survey. Drones. 2025; 9(8): 577. doi: 10.3390/drones9080577
17. Kostek AA, Lößle F, Wickersheim R, et al. Experimental investigation of UAV rotor aeroacoustics and aerodynamics with computational cross-validation. CEAS Aeronautical Journal. 2024; 15(3): 643–658. doi: 10.1007/s13272-023-00680-z
18. Sagaga J, Lee S. High-Fidelity Computational Study of Aerodynamic Noise of Side-by-Side Rotor in Full

Configuration. Journal of Sound and Vibration. 2024; 592: 118607. doi: 10.1016/j.jsv.2024.118607
19. Little DS, Majdalani J, Hartfield RJ, et al. Improved prediction of propeller tonal noise through integration of Hanson's model into a modern surface-vorticity panel code. Aerospace Science and Technology. 2025; 164: 110381. doi: 10.1016/j.ast.2025.110381
20. CFD Support. Acoustic Benchmark Propeller DJI 9450. CFD Support; 2022.
21. Leishman JG. Introduction to Aerospace Flight Vehicles. ERAU EaglePubs; 2022.
22. Veerasamy D, Atkin CJ, Ponnusami SA. Aerofoil wake-induced transition characteristics on a flat-plate boundary layer. Journal of Fluid Mechanics. 2021; 920: A29. doi: 10.1017/jfm.2021.452
23. Turhan BB, Jawahar HK, Bowen L, et al. Turbulent Flow Impact on the Acoustic and Aerodynamic Performance of Overlapping Propellers. In: Proceedings of the 30th AIAA/CEAS Aeroacoustics Conference; 4–7 June 2024; Rome, Italy. doi: 10.2514/6.2024-3422
24. Wan Mohamed WM, Ravindran NP, Rajendran P. A CFD Simulation on the Performance of Slotted Propeller Design for Various Airfoil Configurations. CFD Letters. 2021; 13(3): 43–57. doi: 10.37934/cfdl.13.3.4357
25. Roy S, Das B, Biswas A. Influence of Camber Ratio and Thickness Ratio on the Airfoil Performance. In: Pande KM, Misra RD, Patowari PK, et al (editors). Recent Advances in Mechanical Engineering, Lecture Notes in Mechanical Engineering. Springer Singapore; 2021. pp. 729–737. doi: 10.1007/978-981-15-7711-6_72
26. Zheng ZC, Li W, Wang FY, et al. Influence of Vortex Core on Wake Vortex Sound Emission. Journal of Aircraft. 2007; 44(4): 1369–1377. doi: 10.2514/1.27077